

Regional application of an ecosystem production model for studies of biogeochemistry in Brazilian Amazonia

CHRISTOPHER S. POTTER,^{1*} ERIC A. DAVIDSON,² STEVE A. KLOOSTER,¹
DANIEL C. NEPSTAD,² GUSTAVO H. DE NEGREIROS³ and VANESSA BROOKS¹

¹Ecosystem Science Branch, NASA-Ames Research Center, Mail Stop 242–4, Moffett Field, CA 94035, ²Woods Hole Research Center, PO Box 296, Woods Hole, MA 02543, ³College of Forest Resources, University of Washington, Seattle, WA 98195

Abstract

The degree to which primary production, soil carbon, and trace gas fluxes in tropical forests of the Amazon are limited by moisture availability and other environmental factors was examined using an ecosystem modelling application for the country of Brazil. A regional geographical information system (GIS) serves as the data source of climate drivers, satellite images, land cover, and soil properties for input to the NASA Ames-CASA (Carnegie-Ames-Stanford Approach) model over a 8-km grid resolution. Simulation results lead us to hypothesize that net primary production (NPP) is limited by cloud interception of solar radiation over the humid north-western portion of the region. Peak annual rates for NPP of nearly 1.4 kg C m⁻² year⁻¹ are localized in the seasonally dry eastern Amazon in areas that we assume are primarily deep-rooted evergreen forest cover. Regional effects of forest conversion on NPP and soil carbon content are indicated in the model results, especially in seasonally dry areas. Comparison of model flux predictions along selected eco-climatic transects reveal moisture, soil, and land use controls on gradients of ecosystem production and soil trace gas emissions (CO₂, N₂O, and NO). These results are used to formulate a series of research hypotheses for testing in the next phase of regional modelling, which includes recalibration of the light-use efficiency term in NASA-CASA using field measurements of NPP, and refinements of vegetation index and soil property (texture and potential rooting depth) maps for the region.

Keywords: Amazon, biogeochemistry, ecosystem modelling, trace gases, transects

Received 2 April 1997; revised version accepted 5 July 1997

Introduction

Tropical ecosystems are major locations for biogenic exchange of greenhouse gases (e.g. CO₂, CH₄, N₂O), with the atmosphere, and potentially for emission of reactive tropospheric gases (NO_x, CO, and volatile organic carbon compounds). For example, evidence from field measurements supports the hypothesis that tropical forests are the most important global biogenic source of N₂O and a major source of soil NO (Davidson 1991; Keller & Reiners 1994). Nevertheless, considerable uncertainty remains as to how seasonal rainfall patterns and timing interact with soils and land cover types to control carbon fluxes and emissions of the major trace gases in the Amazon region (Nepstad *et al.* 1994; McKane *et al.* 1995).

Understanding the coupling of ecosystem moisture,

carbon, and nutrient flows is a key to advancements in tropical forest biogeochemistry, and to biosphere-atmosphere coupling. The movement and storage of rainfall through tropical plant canopies and soils affects many important ecosystem processes (Roberts & Cabral 1993; Grace *et al.* 1995), including evapotranspiration, net primary production (NPP), and soil microbial activity that can produce or consume atmospheric trace gases. Changes in the presumed natural balance between NPP and soil heterotrophic respiration may occur as a result of physical or chemical conditions of the ecosystem (Nobre *et al.* 1996), but there is a lack of evidence to suggest how and where this balance is changing most rapidly in the Amazon region.

Land cover change could be altering regional NPP and carbon budgets significantly in tropical environments. Notable expanses of secondary forest may be regenerating

Correspondence: C.S. Potter, tel +1/415-604-6164, fax +1/415-604-4680, e-mail cspotter@gaia.arc.nasa.gov

from disturbance throughout Amazonia. These stands could represent a substantial sink for atmospheric carbon (Lucas *et al.* 1996). However, the interaction of climate variability (including periodic drought), plant moisture use, and land cover change is not well understood with respect to the sustained productivity of vegetation in converted forest lands. Further research is needed to determine the relative tolerance to climate fluctuations of secondary forest, pasture, and crop plants compared to the mature trees they may be replacing (Nepstad *et al.* 1995).

Direct measurements of whole ecosystem fluxes of moisture, carbon, and nitrogen can be difficult and expensive to gather, especially in remote rain forest locations. Consequently, large-scale field studies of terrestrial biogeochemistry are often founded on the principle that development and testing of spatial simulation models are also required to predict patterns and changes in carbon and nutrient cycling dynamics, and to scale-up to regional estimates. Ecosystem simulations can also help identify the types of ground-based measurements that are most needed to test new theories of biogeochemical cycling at intensive field study sites. Ideally, the interaction between modelling and field studies is iterative and frequent (Root & Schneider 1995).

This paper describes results from application of a gridded computer model intended to progressively improve the resolution (both spatial and seasonal) and process-level understanding of biogeochemistry and trace gases emissions in Amazon ecosystems. The model we used, the NASA Ames version of CASA (Carnegie-Ames-Stanford Approach; Potter & Klooster 1997), is notable among the existing simulation models in that it simulates a host of biogenic trace gas fluxes (CO_2 , N_2O , NO , and others) on a regional scale by merging input datasets of satellite 'greenness' index, climate, radiation, vegetation, and soils with simple algorithms for moisture flow and nutrient transformation processes in terrestrial ecosystems. Use of satellite data to drive the CASA model's NPP flux by plant communities is an important feature, because (i) predicted carbon input fluxes are formulated to be consistent with the range of measured rates, and (ii) actual regional patterns for land cover attributes may differ substantially from potential vegetation maps.

Although application of the model over the region of Brazil at spatial resolution of 8-km cannot capture all the localized and transient effects of land use change (including pasture management and secondary forest regrowth) in a statistically significant manner, this ecosystem modelling study does permit a reasonably detailed geographical analysis that demonstrates the potential interactions of relatively extensive land cover classes, rainfall gradients, and soil types in the Amazon during a hypothetical 'average' climate year. Consequently, our

main objective is to use results from our simulation model to help formulate hypotheses that can be tested in tropical field studies, such as the Large Scale Biosphere-Atmosphere Experiment in Amazonia (LBA 1996), and to potentially identify within a geographical context which supporting parameter measurements need to be included in regional research campaigns in order to improve future modelling research.

Background on the model design

The NASA-CASA model includes interactions of several controls on plant production and soil trace gas fluxes: nutrient substrate availability, soil moisture, temperature, soil texture and microbial turnover (Fig. 1). The model has been run globally on a monthly time interval to simulate seasonal patterns in carbon uptake, nutrient allocation, litterfall, soil nitrogen mineralization and CO_2 , N_2O , NO fluxes. Satellite imagery from the Advanced Very High Resolution Radiometer (AVHRR) is used to calculate net primary production (NPP), based on the concept of light-use efficiency described by Monteith (1972). The coupled plant production and soil respiration components of the model are regulated by a common soil moisture submodel. The reader is referred to the Potter *et al.* (1993, 1996) and Potter & Klooster (1997) for a more detailed description of the general model design and specific algorithms.

The soil submodel in this version of NASA-CASA simulates carbon and nitrogen cycling using a set of compartmental difference equations based on a simplified version of the CENTURY model (Parton *et al.* 1987, 1992). Soil heterotrophic respiration, carbon and nitrogen fluxes are controlled using series of nondimensional indices related to air temperature, soil moisture, litter substrate quality (N and lignin contents), and soil texture. Nitrogen transformations which lead to substrates for trace gas production are stoichiometrically related to C flows (Fig. 2). Nitrogen fluxes from litter and soil to microbial pools and from microbial pools back to soil pools occur in proportion to microbial C assimilation rates so that prescribed C-to-N ratios for the various recipient organic matter pools are maintained (Parton *et al.* 1992). Litter decomposition is slower where substrate lignin-to-nitrogen ratio is high. Soil texture controls microbial turnover rates (lower in fine textured soils), and regulates the fraction of carbon lost as CO_2 from soil microbes during transfer to the SLOW pool (i.e. the pool with turnover time of a decade or more), which decreases as the soil silt plus clay content increases.

Gross N mineralization is distinguished as the total N released during decomposition of litter and soil organic matter. Under non nutrient-limiting conditions, the amount of N released during mineralization is propor-

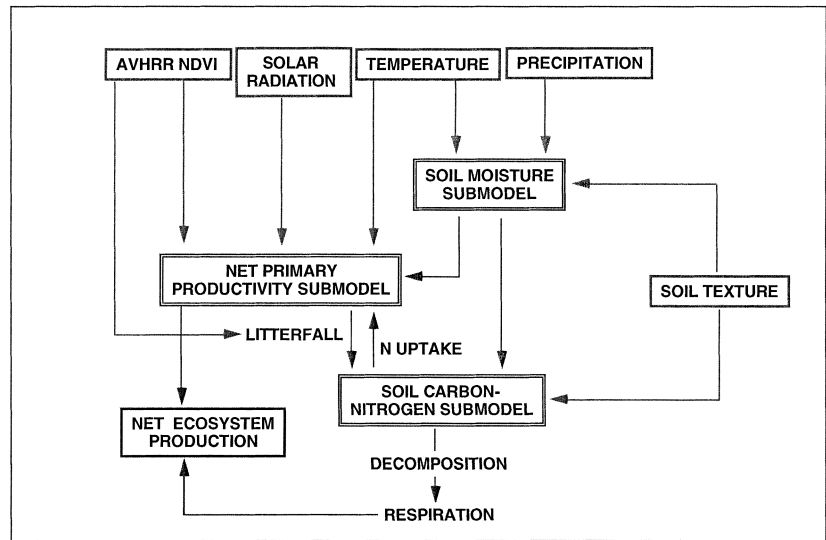


Fig. 1 Framework for driver variables and submodel coupling in the NASA-CASA model.

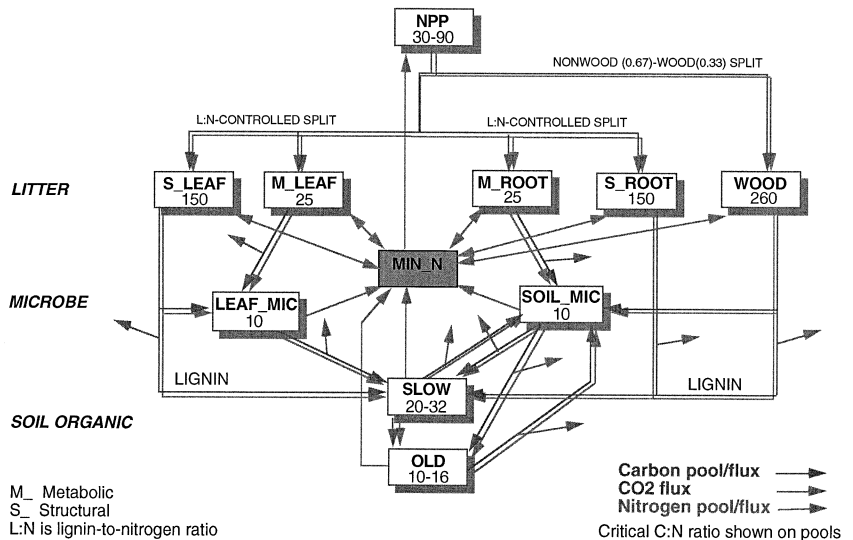


Fig. 2 Litter and soil C and N transformations which lead to substrates for trace gas production in the NASA-CASA model. Carbon pools are outlined in black and labelled with C-to-N ratios, C fluxes in solid arrows, CO₂ production in stippled arrows; Nitrogen pools in gray, N fluxes in gray arrows. NPP is split between woody and nonwoody litter fractions. Litter, microbe (MIC) and soil organic (SLOW and OLD) pools make up the nonplant storage of ecosystem C and N. Structural (S) and metabolic (M) pools are shown for leaf and root litter.

tional to CO₂ emission from carbon pools. Gross microbial immobilization occurs at rates necessary to maintain prescribed pool C-to-N ratios. Net mineralization fluxes to the common mineral N pool (MIN_n) are equal to the difference between gross mineralization and immobilization fluxes.

The algorithms in NASA-CASA for nitrogen trace gas emission are based on evidence accumulated from measured fluxes in temperate and tropical settings which suggests that soil water content alone is a fairly reliable predictor of proportional (NO:N₂O:N₂) gas emissions (Davidson 1993; Riley & Vitousek 1995). This assumption was the basis for a global application of the CASA model (Potter *et al.* 1996), in which we tested the hypothesis that variability in the ratio of N₂O:NO emissions over broad spatial gradients depends upon seasonal patterns of soil wetting and drying.

The primary controlling factors used in the CASA

'leaky pipe' model (Firestone & Davidson 1989) for emissions of NO and N₂O are gross rates of N mineralization and an index of water-filled pore space (WFPS; defined as the ratio of volumetric soil water content to total porosity of the soil; Papendick & Campbell 1980). Rates of N mineralization derive from the CASA compartmental model of element cycling among litter, microbe, and soil organic matter pools. As mentioned above, we have used satellite-derived 'greenness' observations to compute plant residue addition as one of the main controlling variables of soil N cycling. Although other factors, such as soil acidity, may affect emissions of N trace gases in some soils, it appears that N availability and soil aeration are the dominant controllers now obtainable for regional model applications.

In the CASA conceptual model (Potter *et al.* 1996), we lump the processes of ammonification and nitrification into combined mineralization fluxes from litter, microbial

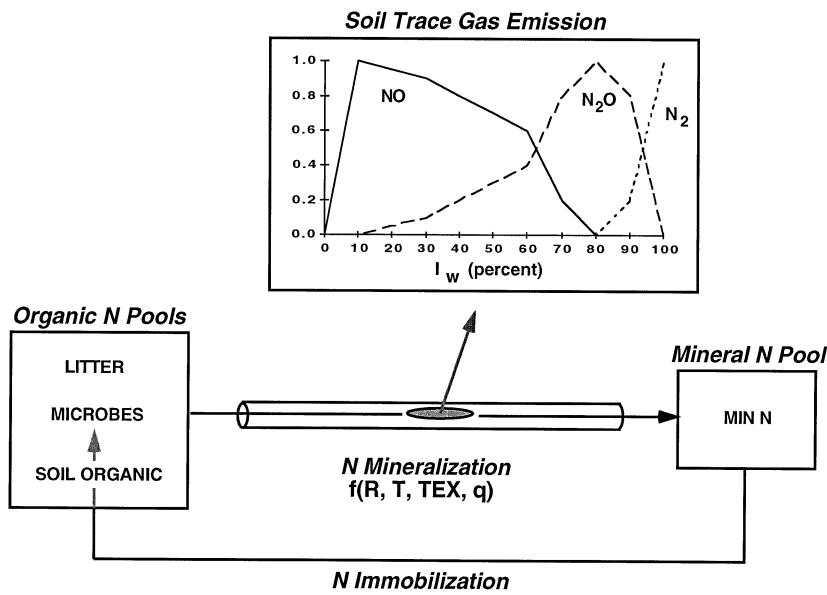


Fig. 3 Schematic representation of the nitrogen trace gas submodel. Gross mineralization of nitrogen from litter and soil N pool is a function of rainfall (R), temperature (T), soil texture (TEX) and substrate quality (q). The scalar for relative production of N trace gases is a function of the WFPS probability index (I_w).

and soil organic matter pools for transfer to a common mineral N pool. For our model design, we represent the proportion of N trace gas ($\text{NO}:\text{N}_2\text{O}:\text{N}_2$) emitted as a byproduct of mineralized N as overlapping functions of WFPS (Fig. 3). This ratio of $\text{NO}:\text{N}_2\text{O}:\text{N}_2$ conceptually represents the size of holes in the N flux 'pipe.' Production and emission of both NO and N_2O occurs at intermediate levels of WFPS. At higher moisture levels where reducing conditions develop, emission of relatively more N_2O is a result of an exponential response to WFPS. NO emission declines as the soil becomes nearly saturated, possibly due to diffusion limitations from sites of production at the intra-aggregate pore space (Schuster & Conrad 1993). Under very wet soil conditions, only production of N_2 occurs. These algorithms are consistent with observed flux measurements and current understanding of process-level regulation of nitrification and denitrification end products (Linn & Doran 1984; Matson & Vitousek 1990; Hutchinson & Davidson 1993).

Development of regional model drivers for Brazil

For this regional model application to the country of Brazil, we used the same NASA-CASA algorithms as for global ecosystem simulations (Potter & Klooster 1997). However, in the place of global 1° inputs, regional datasets (8-km resolution) from a geographical information system (GIS) were used as model drivers and land surface parameter files. We assembled a complete set of GIS raster coverages to serve as model-compatible inputs, including monthly rainfall and surface air temperature, surface solar radiation, soil texture, land cover type, and

satellite vegetation index for the country of Brazil and, in some cases, for the larger Amazon region.

All raster maps were gridded at 8-km spatial resolution in an equal area projection. In terms of single grid cell size (64 km^2), this produces an improvement in spatial resolution of more than 150 times, compared to the global 1° ($\approx 10^4 \text{ km}^2$ cell size) data drivers for the model. The coastal boundary line file used as a base to geo-reference the 8-km map set was taken from the Digital Chart of the World (DCW 1993).

Satellite Vegetation Index

We obtained the monthly composites for the year 1990 of Normalized Difference Vegetation Index (NDVI) from the Advanced Very High Resolution Radiometer (AVHRR), which is available from the NOAA/NASA Pathfinder AVHRR Land (PAL) program at NASA Goddard Space Flight Center's (GSFC) Distributed Active Archive Center (DAAC). Complete AVHRR datasets are produced from NOAA Global Area Coverage (GAC) Level 1B data, and consist of reflectances and brightness temperatures derived from the five-channel cross-track scanning AVHRR aboard the NOAA Polar Orbiter 'afternoon' satellites (NOAA-7, -9, and -11). DAAC references by Agbu & James (1994) and Kidwell (1991) provide more information on the derivation and potential use of these NDVI products.

Monthly composite datasets are designed to remove much of the contamination due to cloud cover present in the daily AVHRR datasets (Holben 1986). To generate a composite dataset, eight to 11 consecutive days of data are combined, taking the observation for each 8-km bin

from the date with the highest NDVI value. Only data within 42 degree of nadir are used in the composite to minimize spatial distortion and bi-directional effect biases at the edge of a scan. A Rayleigh correction is calculated and applied using a standard radiative transfer equation and methodology, which follows the work of Gordon *et al.* (1988).

Having obtained 12 months of PAL files for South America NDVI, we ran a low-pass filter over the data to remove several narrow lines of anomalous high values which are presumably a result of compositing. The filter routine computes the mean of six nearby grid cell values (located two rows and three columns above each cell location), and compares this average to the actual cell value. If the difference between the original cell value and the average of the values above that cell is greater than 200 units, then the value of that cell is replaced by the average of the nearby cell values. Typically, less than 25% of the NDVI values over the entire regional land area required modification with this filtering step.

Although PAL composite dataset are produced expressly for studies of temporal and interannual behaviour of surface vegetation, subsequent processing is recommended if a more complete cloud-free signal is required. Consequently, we applied Fourier smoothing algorithms (FA) developed by Los *et al.* (1994) for AVHRR datasets to further remove anomalous NDVI signals due presumably to remaining cloud cover interference. Settings for this FA correction include three temporal harmonics and a weighted Fourier transform, i.e. values which fall above the Fourier curve are given more weight than values below the curve. This assumes that higher NDVI values are more likely to be correct than low NDVI values which could occur during periods of cloud or smoke formation. The FA algorithm modified mean annual NDVI values by more than + 10% of their original values in approximately four out of every 10 grid cells in the region.

Unlike in earlier versions of the CASA-Biosphere model (Potter *et al.* 1993; Potter & Klooster 1997), we avoided in this NASA-CASA version use of AVHRR-NDVI datasets with interpolation and reconstruction features added (Sellers *et al.* 1994). The main justification for this decision is based on lack of verification of the NDVI reconstruction algorithm for the extent of tropical evergreen forest.

From these monthly FA-NDVI datasets for South America, we applied empirical algorithms described by Potter *et al.* (1993) to compute second-level model drivers for the fraction of intercepted photosynthetically active radiation (FPAR) and the fraction of yearly litterfall per month at each 8-km grid cell.

Land cover type

The land area within the country of Brazil covers $\approx 8.63 \times 10^6$ km². For land cover characterization,

we aggregated 39 cover classes developed for South American vegetation by Stone *et al.* (1994) from analysis of 1-km AVHRR -NDVI patterns, into four general classes represented in the global land cover classification scheme of DeFries & Townshend (1994). Of the four general land cover classes represented at 8-km grid cell resolution (Fig. 4a), broadleaf forest is the most common (48% of total area), followed by wooded grassland and savanna (32%), cultivated lands (15%), and all other cover types combined, including wetlands, river ways, and bare ground (5%). The vegetation map of Stone *et al.* (1994) is reported to have an overall accuracy of 90%, based on ground-truth analysis of all 39 cover classes.

By aggregating all agricultural areas (Stone *et al.* 1994) into a common 'cultivated' class, we did not attempt to account for differences in stand age, crop type, or agro-soil system management in the model algorithms for plant and soil biogeochemistry. Furthermore, although important differences in physiology and biogeochemistry could be related to forest stand age, we did not attempt to distinguish between primary, secondary, or recently cleared forest types with respect to this initial application of the NPP algorithm coefficients. In short, we applied the same NPP algorithm coefficients developed from the global version of the NASA-CASA model (Potter & Klooster 1997) to the relatively undisturbed forests or savannas and to their respective 'cleared or degraded' cover categories (Stone *et al.* 1994). This means that any differences in model results reported for different forest cover types (e.g. predominantly moist evergreen vs. seasonally deciduous forests; Stone *et al.* 1994) would not be attributable to CASA internal model settings in the general land cover groups defined above, but instead to patterns in NDVI, climate, or soils inputs to the model.

Model parameters that are assigned according to the four general land cover types include leaf litter nitrogen:lignin content (Potter & Klooster 1997), decomposition rates of soil carbon in cultivated soils, and plant rooting depth. For the broadleaf forest class, rooting depth is set uniformly to 2-m, whereas in the other three land cover classes, it is set uniformly to 1-m.

Soil texture and carbon content

Soil attribute maps for Brazil were created by interpolation of soil profile data available for more than 1000 Amazon soil pits (Negreiros & Nepstad 1994), assembled during the RADAMBRASIL campaign (MME 1981). We used these soil profile measurements of particle size fractions (sand:silt:clay) in combination with the RADAMBRASIL soils map for Brazil which defines 19 generalized soil groups cross-referenced to the pit profile entries. The regional soils map was used as the basis to interpolate pit profile attributes within soil groups using the nearest-

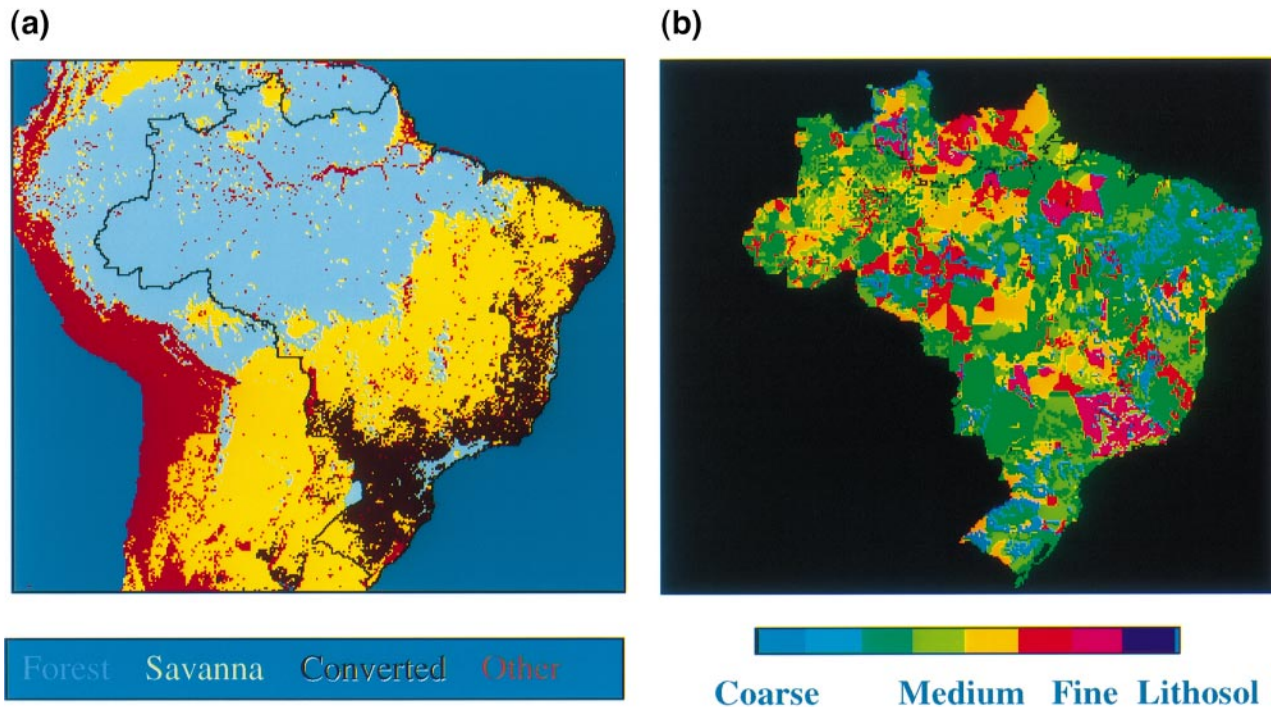


Fig. 4 Classification of (a) land cover types and (b) soil texture groups used in model simulations for Brazil.

neighbour similarity of profile soil classification to the matching soil group. The procedure was used to produce soil attribute maps for texture class (Fig. 4b), along with carbon and nitrogen content, and pH (not shown). Soil texture classes were assigned on the basis of estimated clay content (FAO 1971). We consider these maps to be most accurate westward of 42° W and northward of 20° S.

This method of soil mapping indicates that, on average, oxisols have a higher clay content in surface horizons than any other soil group in the Amazon, including ultisols (see Table 1). The most sandy soil groups are the spodosols, alfisol/mollisols, psammets, and entisols. Vertisols typically fall into a medium texture class. A separate soil group for lithosols (10-cm rooting depth) is included in the map.

Monthly rainfall and surface air temperature

Monthly mean climate maps for South America were obtained from ZedX, Inc. (Boalsburg, PA, USA). We regridded the original files from 10-km spatial resolution to our nominal 8-km cell size using a nearest neighbour algorithm. These average climate datasets are generated based on long-term (1961–90) records from 98 weather stations in Brazil, which are part of the 'Global Historical Climatology Network' at the Carbon Dioxide Information Analysis Center, Oak Ridge National Laboratory. The spatial interpolation is done by three-dimensional linear regression. Accuracy of the resulting climate maps are

checked by percentage absolute difference analysis with comparison to original station values.

Solar surface radiation

Solar radiation datasets, averaged for the late-1980s, were computed surface irradiance from the International Satellite Cloud Climatology Project (ISCCP) (Bishop & Rossow 1991). This dataset combines estimates of atmospheric optical depth from the ISCCP with calculations from a simplified general circulation model (GCM) transfer scheme to estimate monthly surface irradiance. The data are documented to have an accuracy of 9 W m⁻² on a daily basis and less than 4% overall bias in the 17-day mean relative to ground measurements. We regridded these monthly files to 8-km spatial resolution using a nearest neighbour algorithm. For use in this NASA-CASA's Amazon application, we smoothed the resulting datasets by assigning the mean of a 16 × 16 matrix around each grid cell to the new grid cell value.

Regional model results and interpretation

The NASA-CASA model was run over the Amazon region for a 100-year simulation to near-steady state conditions with respect to soil moisture and carbon pools which were initialized at zero. We note that results from this 'average climate year' model scenario are not intended to reflect interannual variability, for example,

Table 1 Soil texture classification within soil groups (all data values are in percentage land area)

Soil group ^b	Soil texture class ^a					No data
	Coarse < 20%	Coarse–Medium < 30%	Medium < 48%	Medium–Fine < 67%	Fine ≥ 67%	
Latosolos (Oxisol)	32.5	16.2	25.2	16.9	9.2	0.0
Terras Roxas Estruturadas (Alfisol)	5.1	12.5	63.0	18.5	1.0	0.0
Solos Podzolicos (Ultisol)	53.5	28.7	15.8	1.9	0.1	0.0
Podzol (Spodosol)	92.8	4.1	1.7	0.9	0.1	0.3
Brunizens (Mollisol/Alfisol)	1.1	6.2	71.9	20.8	0.0	0.0
Solos Brunos Nao Calcicos (Alfisol/Mollisol)	96.4	2.9	0.7	0.0	0.0	0.0
Planosolos (Alfisol/Ultisol/Mollisol)	95.3	3.9	0.8	0.1	0.0	0.0
Solonetz-Slodizado (Alfisol/Mollisol)	96.8	1.3	1.3	0.7	0.0	0.0
Solos Salinos (Aridisol)	48.7	37.3	8.8	4.6	0.7	0.0
Cambissolos (Inceptisol)	18.3	51.4	17.7	12.4	0.2	0.0
Lateritas Hidromorficas (Oxisol/Ultisol)	57.6	23.7	17.0	1.5	0.0	0.1
Solos Gley (Inceptisol)	22.3	22.9	43.4	9.7	1.6	0.2
Solos Arenoquartzosos (Psamments/Entisol)	94.9	3.3	1.1	0.5	0.1	0.1
Vertissolos (Vertisol)	15.7	22.1	60.5	1.7	0.0	0.0
Regossolos (Entisol)	98.1	1.2	0.7	0.0	0.0	0.0
Solos Alluviais (Entisol)	58.5	13.5	18.2	9.6	0.0	0.1
Concrecionarios Lateriticos (Oxisol)	27.1	68.8	3.2	0.7	0.3	0.0
Rivers and other water	34.0	17.3	15.7	5.0	3.0	25.1

^aDefinitions of texture classes (FAO 1971) are based on clay content shown in percentage.

^bUSDA soil group assignments (in parentheses) follow systems described by Birkeland (1974) and Moraes *et al.* (1995) using the Brazilian classification.

an El Niño event, when rainfall can decline substantially below long-term average amounts.

Moisture balance

Potential evapotranspiration (PET), computed according to the method of Thornthwaite (1948), is fairly uniform throughout the year across the Amazon Basin region. Daily PET is typically estimated between 3 and 4.5 mm, with maximum fluxes of about 5.2 mm d⁻¹ in the extreme eastern areas of the Basin during the months of September–October. This estimated range is consistent with reported evapotranspiration measurements from Amazon forests (Shuttleworth 1988; Roberts & Cabral 1993; Nepstad *et al.* 1994; Jipp *et al.* 1997). Geographically, PET increases slightly moving from west to east across the basin, and decreases gradually moving north to south.

There are, admittedly, important potential limitations to the Thornthwaite method for estimation of PET. Although air surface temperatures may rise little from wet to dry seasons (presumably explaining the relatively low variation in our estimated PET across seasons), radiation can vary greatly, which may increase actual ET during the dry season. It is plausible that a simple water

balance model tends to underestimate the role of drought over the region.

Based on the model's moisture balance equations (Potter & Klooster 1997) run to a steady-state condition with respect to mean climate conditions, we estimated seasonal WFPS status of soils. Model results suggest that precipitation rates over the Amazon basin are sufficient to maintain predicted WFPS at > 50% over most of the tropical forest region throughout the year, regardless of soil texture. As rainfall decreases over the seasonally dry (but mostly evergreen) forest areas of the eastern Amazon basin from June to October, surface soil layers can dry out to estimated WFPS of 30–40%. Surface soils can dry down to below 30% WFPS in areas of coarse–medium texture (low moisture-holding capacity) or in areas mapped as shallow lithosols (Fig. 4b).

Plant production

Comparison of the model's average estimated NPP of forest and woodland cover types with their converted or secondary analogs imply regional effects of forest conversion on annual production in the Amazon Basin. These comparisons are quantified in the section that

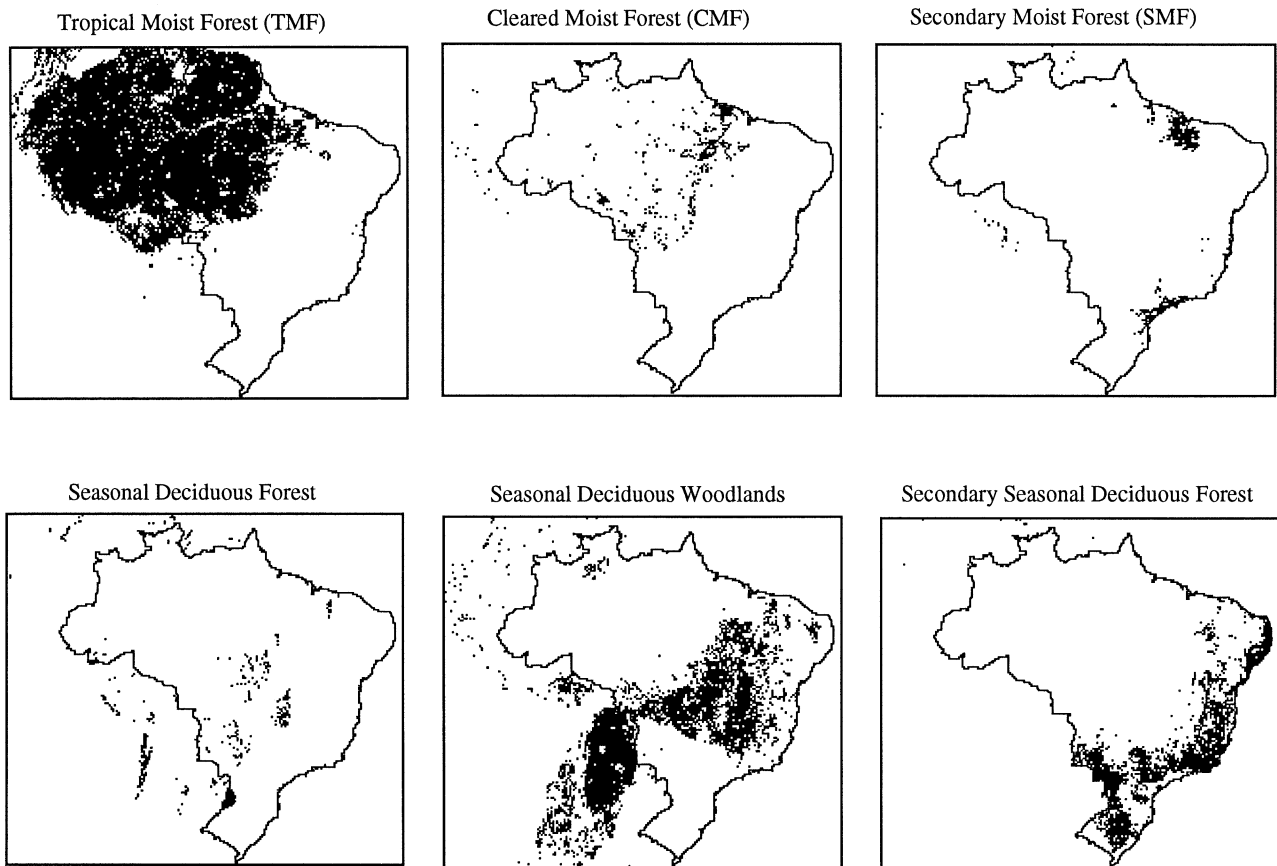


Fig. 5 Regional distribution of forest and woodland cover types from the classification of Stone *et al.* (1994). Grouping into generalized land cover classes for NASA-CASA settings is shown in Table 2a.

follows. We presume that the most straightforward comparisons will be among only evergreen forest types, or among only drought-deciduous woodland types (Fig. 5), mainly because we cannot completely rule out the confounding effects of soil and climate among results for forest types that differ substantially in seasonal phenology.

Tropical moist forest

In the most productive cover class, estimated NPP exceeds $1200 \text{ g C m}^{-2} \text{ y}^{-1}$ (Fig. 6) on average throughout the extensive tropical moist forest (TMF, Stone *et al.* 1994). This is evergreen forest that covers over 40% of all Brazil (Fig. 5), and over 70% of the legal Amazon basin (as delineated geographically by Skole & Tucker 1993).

According to the classification by Stone *et al.* (1994), 'cleared' moist forest (CMF) covers slightly more than 5% of the legal Amazon area (Fig. 5), and might be considered the dominant land use change within the Amazon forest region. This CMF class covers about the same amount of land ($258\,000 \text{ km}^2$) identified in the Amazon 'crescent' of deforestation by Skole & Tucker

(1993) using Landsat satellite data. We note that cells classified by Stone *et al.* (1994) as CMF are predominantly located in locations also defined by Skole & Tucker (1993) as 20–80% deforested.

Of all cells in the CMF class, our model estimates that about 13% has NPP lower than $1000 \text{ g C m}^{-2} \text{ y}^{-1}$, and a small area (about 1%) has NPP lower than $500 \text{ g C m}^{-2} \text{ y}^{-1}$, suggesting the locations of fairly recent deforestation or some other interruption in forest cover. These areas are scattered widely across eastern Pará, Mato Grosso, and into Rondônia, where large cattle ranches are commonly located. In comparison, only 3% of the (relatively undisturbed) TMF class in Brazil has NPP lower than $1000 \text{ g C m}^{-2} \text{ y}^{-1}$.

At the spatial resolution of 8-km, we detect a small but notable overall difference in mean annual NPP (g C m^{-2}) between areas classified as TMF (4% higher), compared to CMF areas (Table 2a). This could be attributable, at least in part, to 10% higher rainfall on average in the TMF areas in western Amazonia. In addition, the ratio of the number of grid cells falling into the soil type categories of oxisols vs. ultisols (as defined by the MME 1981) is higher in the CMF (1.6–1) than in the relatively

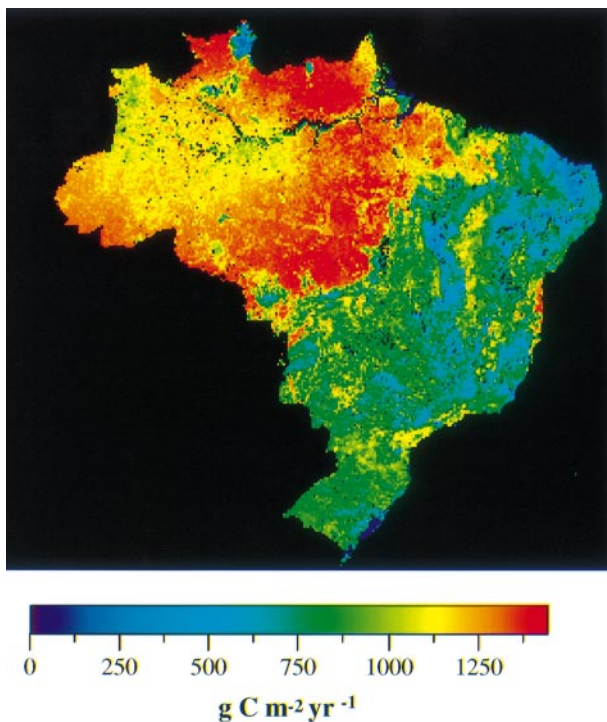


Fig. 6 Net primary production estimated at 8-km cell resolution by the NASA-CASA model for Brazil, c. 1990.

undisturbed TMF (1.1–1). For the entire region of Brazil, vegetation growing on oxisols is slightly less productive, on average, than vegetation growing on ultisols (Table 3). The covarying effect of soil texture with soil type is considered later in this section.

Within both the relatively undisturbed TMF and the CMF classes, annual productivity estimated by the model is shown to vary with length of the dry season, which we define as the total number of months during a year with long-term average rainfall less than 45 mm mo^{-1} . Notably, annual productivity within the relatively undisturbed TMF class appears to be less sensitive to extended dry season. For example, by controlling for seasonal rainfall patterns, we find that within the TMF class, the percentage of grid cells with annual NPP higher than 1000 g C m^{-2} is 99% for those with a dry season length of one month, decreasing to 93% for those with three months, and to 28% for those with five months dry season length. In comparison, we find that within the CMF class, the percentage of grid cells with annual NPP higher than 1000 g C m^{-2} is 97% for those with a dry season length of one month, decreasing to 75% for those with three months, and 0% for those with five months dry season length.

This pattern, generated primarily by model response to regional data drivers of NDVI and seasonal rainfall, leads us to hypothesize that the plant communities

replacing moist forests in the CMF areas are less productive under conditions of extended dry duration than are relatively undisturbed TMF communities. Pasture plants and, perhaps, annual crops planted in areas of cleared rain forest are less tolerant of drought and less capable of tapping deep soil moisture supplies than the forest tree species that they replace (Nepstad *et al.* 1994, 1995). It appears therefore, that if extreme dry events become more prevalent in Amazonia in coming years, forest conversion could exacerbate an already destabilizing climate effect on regional NPP.

In addition to the CMF class, Stone *et al.* (1994) included a category for secondary moist forest (SMF), presumably regenerating from conversion, mixed with some agriculture, in their land cover classification scheme (Fig. 5). This SMF class covers almost 2% of the legal Amazon area. The original (primary) vegetation of these areas is identified largely as 'floresta ombrofila densa' and semideciduous seasonal forest in the vegetation map of Brazil (IBGE/IBDF 1988). We find a relatively large difference in annual NPP between areas classified as TMF (13% higher), compared to those classified as SMF. This difference cannot be attributed in a general sense to differences in soil texture or type (oxisol vs. ultisol) of these different forest classes. However, in addition to potential land use effects on estimated FPAR from NDVI, the pattern may be related to lower (20%) mean annual and seasonal rainfall in the SMF areas. On the other hand, SMF areas receive 3% higher solar radiation on average over the season, which may offset moisture deficits somewhat with respect to predicted NPP.

It should be noted that, with respect to our ecosystem model design, there remains a high level of uncertainty concerning moisture controls on NPP in seasonally dry evergreen forest areas. Nepstad *et al.* (1994) estimated that half of the closed forest of the Brazilian Amazon depend on deep root systems to maintain green canopies during the dry season. Evergreen forests of the eastern Amazon can sustain evapotranspiration by absorbing water from the soil to depths of more than 8 m. Our default model setting permits rooting to 2 m depth in all forest classes, regardless of stand age or disturbance. Hence, improvements in the large-scale modelling of below-ground biomass dynamics and water balance will depend in part on more dependable information for forest rooting depths over the entire region. For now, we can address the issue of root depth as a model sensitivity analysis (see subsequent section of this paper).

Seasonal deciduous forests

Compared to the areas mapped by Stone *et al.* (1994) as TMF, seasonal deciduous forest areas (found largely outside the continuously moist Amazon zone), are estim-

Table 2a Carbon fluxes and pool sizes estimated by NASA-CASA as averages for land cover classes (Stone *et al.* 1994)

Land cover class	Area covered (Percent)	Area covered (10 ⁶ km ²)	NPP g C (m ⁻² y ⁻¹)	NPP (Pg C y ⁻¹)	GSNF ^a (g C m ⁻²)	Soil C total ^b (g C m ⁻²)	Soil C total ^b (Pg C)	Soil C SLOW (g C m ⁻²)	Soil C SLOW (Pg C)
Rivers (and other water) ⁴	1.9	0.166	–	–	–	–	–	–	–
Tropical Moist & Semi-Deciduous Forest ¹	41.5	3.583	1232.4	4.41	66.6	15475	55.4	3041.0	10.89
Cleared Tropical Moist Forest ¹	3.0	0.258	1178.5	0.30	87.4	14305	3.7	2931.2	0.76
Savanna/Grasslands and Pasture ²	8.0	0.694	887.7	0.62	110.1	10046	7.0	2347.8	1.63
Wet Vegetation/Mixed ⁴	0.6	0.053	–	–	–	13855	–	–	–
Unclassified ⁴	1.0	0.086	–	–	–	10343	–	–	–
Cerrado and Seasonal Deciduous Woodlands ²	15.6	1.343	845.4	1.14	93.6	11650	15.6	2308.4	3.10
Bamboo-dominated Forest ¹	0.1	0.009	1281.9	0.01	48.9	11039	0.1	3347.2	0.03
Secondary Tropical Moist Forest w/ Agriculture ¹	2.4	0.204	1078.2	0.22	124.7	8950	1.8	2969.0	0.60
Pantanal Grassland (seasonally flooded) ⁴	0.4	0.031	–	–	–	21171	–	–	–
Tropical Seasonal Deciduous Forest ¹	1.4	0.124	963.2	0.12	96.2	14835	1.8	2571.4	0.32
Agriculture ³	0.1	0.010	706.5	0.01	117.9	7502	0.1	773.0	0.01
Gallery Forests ²	0.2	0.021	1093.3	0.02	70.3	10602	0.2	2638.1	0.05
Tropical Open Forests (mixed) ²	0.5	0.046	1067.5	0.05	87.0	11539	0.5	2621.8	0.12
Cerrado (woodlands) converted ²	0.6	0.053	764.2	0.04	97.0	16686	0.9	2092.1	0.11
Grasslands or Savanna w/ Agriculture ²	1.2	0.102	864.7	0.09	109.1	10223	1.0	2360.4	0.24
Xerophytic Woodlands (Caatinga) ²	3.7	0.318	736.0	0.23	115.3	7652	2.4	2058.9	0.65
Converted Xerophytic Woodlands (Caatinga) ²	2.6	0.222	653.9	0.15	112.3	7441	1.7	1949.0	0.43
Secondary Seasonal Deciduous Forest w/ Agriculture ³	12.6	1.090	712.8	0.78	126.0	7931	8.7	861.9	0.94
Urban and converted lands ³	0.0	0.001	533.1	0.00	114.5	6603	0.0	651.4	0.00
Converted Tropical Seasonal Deciduous Forest ¹	0.2	0.020	593.0	0.01	136.1	6793	0.1	720.4	0.01
Mixed Pine w/ Secondary Forest & Agriculture ²	2.2	0.192	893.4	0.17	165.3	8400	1.6	1216.9	0.23
Cool Deciduous Forest ⁴	0.0	0.002	13.7	0.00	12.0	5481	0.0	7.2	0.00
Total	100.0	8.627	–	8.37	–	–	105.6	–	20.14

Generalized land cover classes for NASA-CASA simulations are shown as ¹broadleaf forest; ²wooded grassland and savanna; ³cultivated lands; ⁴other.

^aGrowing season net flux (GSNF) is defined as the cumulative NEP over the period of months for which NEP is positive.

^bGIS dataset.

Table 2b Nitrogen fluxes estimated by NASA-CASA as averages for land cover classes (Stone *et al.* 1994)

Land cover class	Litter N g (N m ⁻² y ⁻¹)	Litter N (Tg N y ⁻¹)	Soil N ₂ O (mg N m ⁻² y ⁻¹)	Soil N ₂ O (Tg N y ⁻¹)	Soil NO (mg N m ⁻² y ⁻¹)	Soil NO (Tg N y ⁻¹)	N ₂ O:NO
Tropical Moist & Semi-Deciduous Forest	13.32	47.72	127.42	0.456	198.02	0.709	0.64
Cleared Tropical Moist Forest	12.74	3.28	103.41	0.027	203.06	0.052	0.51
Savanna/Grasslands and Pasture	9.60	6.66	70.72	0.049	159.65	0.111	0.44
Cerrado and Seasonal Deciduous Woodlands	9.14	12.28	59.79	0.080	159.62	0.214	0.37
Bamboo-dominated Forest	13.86	0.13	104.28	0.001	243.08	0.002	0.43
Secondary Tropical Moist Forest w/Agriculture	11.66	2.37	77.29	0.016	195.77	0.040	0.39
Pantanal Grassland (seasonally flooded)	0.00	0.00	0.04	0.000	0.10	0.000	0.36
Tropical Seasonal Deciduous Forest	10.41	1.29	67.26	0.008	185.11	0.023	0.36
Agriculture	23.56	0.25	126.76	0.001	381.53	0.004	0.33
Gallery Forests	11.82	0.24	67.81	0.001	215.60	0.004	0.31
Tropical Open Forests (mixed)	11.54	0.53	76.04	0.003	200.82	0.009	0.38
Cerrado (woodlands) converted	8.26	0.44	54.63	0.003	143.97	0.008	0.38
Grasslands or Savanna w/Agriculture	9.35	0.95	82.73	0.008	135.55	0.014	0.61
Xerophytic Woodlands (Caatinga)	7.96	2.53	35.43	0.011	155.85	0.050	0.23
Converted Xerophytic Woodlands (Caatinga)	7.07	1.57	27.07	0.006	139.58	0.031	0.19
Secondary Seasonal Deciduous Forest w/Agriculture	23.77	25.93	162.81	0.178	342.35	0.373	0.48
Urban and converted lands	17.78	0.02	184.27	0.000	202.40	0.000	0.91
Converted Tropical Seasonal Deciduous Forest	19.78	0.39	79.82	0.002	349.21	0.007	0.23
Mixed Pine Forest w/Secondary Forest & Agriculture	29.79	5.72	258.10	0.050	390.03	0.075	0.66
Cool Deciduous Forest	0.00	0.00	0.22	0.000	0.59	0.000	0.38
Total		112.29		0.901		1.727	0.52

ated to be 20% less productive for the year, on average (Table 2a). We attribute this difference chiefly to lower annual rainfall (33%), lower FA-NDVI and hence lower predicted FPAR, observed throughout the year in the seasonal deciduous forest areas. Although surface solar radiation is, on average, 5% higher in the seasonal deciduous forests compared to TMF areas, predicted FPAR (from FA-NDVI) is typically 13% lower as a yearly average, and nearly 20% lower during dry months (June–October), a period during which any residual cloud cover interference in the AVHRR-NDVI signal should be minimal. The contribution of persistent, large-scale effects of smoke from biomass burning cannot be ruled out completely.

There are notable differences in mean annual NPP between areas classified as seasonal deciduous forest (Table 2a), and those classified as either secondary seasonal deciduous forest with agriculture, or converted seasonal deciduous forest (26% and 38% lower NPP, respectively). Based on comparison of mean climate values over the relatively undisturbed vs. secondary

cover types, our model results imply that the 26% lower mean NPP in secondary seasonal deciduous forests is not easily attributed to differences in either mean annual rainfall (125 cm vs. 123 cm), dry season duration (3.8 months vs. 1.7 months), or surface solar radiation flux (248 W m⁻² vs. 233 W m⁻²). Similarly, differences soil texture settings are unlikely to account for this large effect on model computations of annual production (Table 4). Rooting depth settings (2-m vs. 1-m, depending on land use class) and differences in FA-NDVI and predicted FPAR values appear to be most important in explaining these differences in model NPP estimates. For example, statistical analysis of results from the NASA-CASA production algorithm over tropical semiarid regions has shown that NDVI greenness alone can account for 30–90% of the variation in yearly NPP (Potter *et al.* 1997).

It appears therefore, that for disturbed seasonal deciduous forest classes in Brazil, land use change may be the major factor affecting predicted NPP. As mapped by Stone *et al.* (1994), secondary seasonal deciduous forest

Table 3 Carbon (pools) and nitrogen fluxes estimated by NASA-CASA as averages for soil groups

Soil group	Area covered Percent	Area covered 10 ⁶ km ²	Bulk density ^a (g cm ⁻³)	NPP (g C m ⁻² y ⁻¹)	GSNF (g C m ⁻²)	Soil C Total ^b (g C m ⁻²)	Soil C Slow (g C m ⁻²)	Litter N (g N m ⁻² y ⁻¹)	Soil N ₂ O (mg N m ⁻² y ⁻¹)	Soil NO (mg N m ⁻² y ⁻¹)	N ₂ O:NO
Unclassified	2.6	0.221	—	—	—	—	—	—	—	—	—
Latosols (Oxisol)	38.4	3.309	1.2	1015.1	93.7	12176	2566.9	13.55	127.81	190.11	0.67
Terras Roxas Estruturadas (Alfisol)	1.6	0.135	1.5	890.0	145.5	14166	1973.4	21.56	228.13	252.59	0.90
Solos Podzolicos (Ultisol)	24.9	2.151	1.5	1067.8	80.6	14887	2425.3	13.71	90.83	232.42	0.39
Podzol (Spodosol)	1.5	0.130	1.3	1024.3	54.1	18069	2066.7	11.28	80.66	179.95	0.45
Brunizens (Mollisol/Alfisol)	0.5	0.041	1.4	815.7	132.9	13227	2396.4	13.56	127.40	190.09	0.67
Solos Brunos Nao Calcicos (Alfisol/Mollisol)	1.2	0.102	1.5	557.9	104.5	6526	1455.5	7.30	18.16	149.07	0.12
Planosols (Alfisol/Ultisol/Mollisol)	1.2	0.101	1.5	586.9	92.4	5929	1184.5	10.77	43.42	198.45	0.22
Solonetz-Flodizado (Alfisol/Mollisol)	0.3	0.029	1.5	627.0	65.3	5618	1286.9	9.09	39.18	168.36	0.23
Solos Salinos (Aridisol)	0.2	0.020	1.4	528.3	75.7	3687	1349.4	6.89	29.52	131.86	0.22
Cambissolos (Inceptisol)	2.7	0.234	1.3	861.2	118.3	10556	1993.1	15.61	110.86	247.66	0.45
Lateritas Hidromorficas (Oxisol/Ultisol)	4.8	0.413	1.5	967.5	70.0	18553	2272.4	10.61	65.39	188.96	0.35
Solos Gley (Inceptisol)	3.5	0.302	1.3	978.1	62.2	16578	2458.9	10.95	99.20	171.35	0.58
Solos Arenoquartzosos (Psamments/Entisol)	6.2	0.533	1.4	834.6	80.4	7267	1901.9	10.07	48.39	184.82	0.26
Vertissolos (Vertisol)	0.1	0.011	1.3	639.2	131.6	17813	1654.3	9.60	41.59	186.84	0.22
Solos Litolicos (Entisol)	6.9	0.593	1.4	860.5	101.9	11353	2225.0	14.49	140.16	186.23	0.75
Regossolos (Entisol)	0.5	0.045	1.4	624.8	91.5	5040	1164.0	12.68	47.02	235.23	0.20
Solos Alluviais (Entisol)	0.6	0.054	1.4	732.5	71.3	12386	1667.5	9.13	66.48	150.00	0.44
Concrecionarios Lateriticos (Oxisol)	0.8	0.072	1.5	817.5	80.7	12249	2127.4	9.13	44.17	177.12	0.25
Rivers and other water	1.5	0.132	—	—	—	—	—	—	—	—	—

^aBulk density assignments follow average values reported by Manrique & Jones (1991) for USDA soil groups.^bGIS dataset.

Table 4 Net primary production averaged within soil groups and texture classes (data values are in $\text{g C m}^{-2} \text{y}^{-1}$; showing means with standard deviations in parentheses)

Soil group	Soil texture class				
	Coarse	Coarse-Medium	Medium	Medium-Fine	Fine
Latosolos (Oxisol)	961.5 (321.7)	943.9 (307.7)	1071.7 (299.2)	1134.1 (292.2)	919.4 (326.3)
Terras Roxas Estruturadas (Alfisol)	828.6 (237.6)	892.6 (206.4)	899.6 (213.5)	867.5 (215.3)	757.7 (221.3)
Solos Podzolicos (Ultisol)	1035.3 (317.9)	1046.9 (290.3)	1171.3 (244.3)	1133.0 (281.9)	994.1 (291.8)
Podzol (Spodosol)	983.1 (347.0)	1036.8 (270.8)	994.94 (345.7)	832.6 (448.1)	1308.5 (19.0)
Brunizens (Mollisol/Alfisol)	842.5 (175.6)	782.1 (212.7)	764.2 (276.3)	813.4 (185.5)	N/A
Solos Brunos Nao Calcicos (Alfisol/Mollisol)	555.7 (189.7)	628.4 (158.8)	570.3 (148.4)	N/A	N/A
Planosolos (Alfisol/Ultisol/Mollisol)	581.8 (238.9)	583.6 (237.7)	604.7 (231.1)	N/A	N/A
Solonetz-Strodizado (Alfisol/Mollisol)	601.9 (358.4)	628.6 (423.7)	639.5 (97.75)	528.0 (67.1)	N/A
Solos Salinos (Aridisol)	606.3 (461.4)	582.2 (455.3)	359.6 (366.8)	553.0 (43.8)	N/A
Cambissolos (Inceptisol)	998.4 (320.3)	868.2 (269.7)	853.1 (282.2)	578.3 (216.3)	780.8 (193.2)
Lateritas Hidromorficas (Oxisol/Ultisol)	951.3 (315.1)	931.8 (411.1)	1019.8 (353.0)	1104.9 (249.5)	N/A
Solos Gley (Inceptisol)	897.9 (470.4)	984.6 (417.0)	992.8 (390.6)	994.2 (410.0)	622.6 (507.9)
Solos Arenoquartzosos (Psamments/Entisol)	828.1 (333.9)	870.2 (302.9)	778.6 (371.2)	741.0 (380.3)	844.6 (81.4)
Vertissolos (Vertisol)	615.1 (275.2)	684.3 (145.2)	607.1 (261.9)	784.3 (263.7)	N/A
Regossolos (Entisol)	621.2 (267.5)	605.4 (312.0)	781.0 (219.3)	N/A	N/A
Solos Alluviais (Entisol)	610.8 (520.2)	978.3 (301.3)	846.9 (331.7)	641.6 (427.2)	N/A
Concrecionarios Lateriticos (Oxisol)	751.4 (275.9)	823.5 (267.0)	1057.3 (224.1)	1122.3 (209.4)	868.0 (205.7)
Rivers and other water	719.2 (539.1)	749.8 (512.7)	910.9 (493.3)	796.4 (540.4)	444.3 (492.7)

covers a very broad area (almost 13% of the country) along the extreme eastern side of Brazil from near Fortaleza in the north, south toward Rio de Janeiro, and then out across the extreme southern section of the State of Mato Grosso and also well into Rio Grande do Sul. This disturbed land cover type is classified in the vegetation map of Brazil (IBGE/IBDF 1988) as originally semi-deciduous seasonal forest mixed with cerrado.

Savannas

Annual NPP estimates in relatively undisturbed savannas and seasonal deciduous woodlands (i.e. cerrado areas), which together cover over 25% of Brazilian land area (Stone *et al.* 1994), averages about 30% lower than for TMF and 12% lower than for seasonal deciduous forest areas (Table 2a). This pattern is explained to a substantial degree by average length of the dry season in each vegetation class (Fig. 7). When all land cover classes defined as converted or degraded by Stone *et al.* (1994), most of which fall below the estimated regression line, are excluded from our regression analysis, we find that the relationship between mean annual NPP and length of the dry season is highly significant ($r^2 = 0.6$; $P = 0.02$).

Soil texture and type

The effect of soil texture on annual NPP appears to vary by soil group (Table 4). For example, average NPP

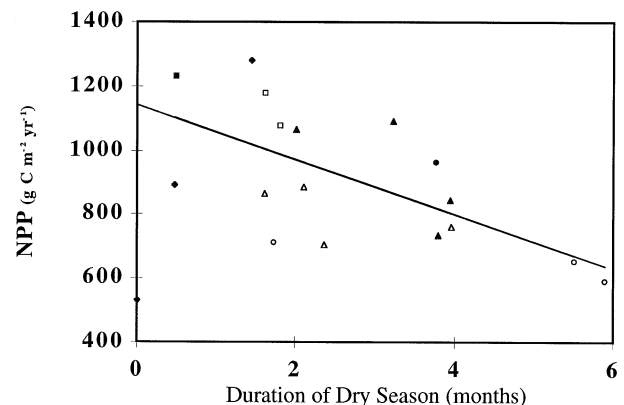


Fig. 7 Average change in net primary production with duration of the dry season for vegetation classes defined by Stone *et al.* (1994). Solid line is the linear regression result. Symbol definitions: \square tropical moist forest, \circ seasonal deciduous forest, Δ savanna or woodland, \diamond other forest type. Filled symbols indicate the relatively undisturbed cover type class, whereas open symbols indicate a converted or disturbed cover type.

estimated in areas classified as predominantly oxisols tends to be lower where coarse texture surface horizons occur, compared to areas classified as predominantly coarse texture ultisols. The difference in annual production is not as great between these two soil groups where medium-fine texture surface horizons are located. NPP is higher in both groups for medium-fine texture soils, compared to coarse texture soils. In areas mapped as

inceptisols, coarse texture soils are more productive on average than fine texture soils, whereas within other soil groups (e.g. spodosols and psamments), soil texture does not appear to affect estimated NPP in any consistent fashion. Soil depth setting is an important controller of estimated production patterns. We note that NPP at grid cells mapped to shallow soil type (lithosols) is estimated to decline substantially shortly after the onset of the dry season (regional data not shown).

It should be stated that our intent in using broad soil groups to stratify model results is to investigate whether the modelled NPP, as influenced by observed NDVI and climate, reveals a pattern that happens to correspond to soil order. No cause and effect relationship is implied at this stage of analysis, although it is possible that soil type and fertility is important for productivity of pastures and regrowth patterns of secondary forests. Nevertheless, the distinction among classes of NPP may occur mainly at the level of soil taxonomy where, for example, eutrophic and dystrophic soils are identified within both ultisols and oxisols.

Soil respiration and net ecosystem production

Annual flux of carbon as CO₂ from soil microbial respiration (R_s) is assumed to be equal to annual NPP for this quasi steady-state model application. Nevertheless, seasonal trends in net ecosystem production (NEP), which is equal to $NPP - R_s$, can be examined. Our model computes a growing season net flux (GSNF) at every 8-km grid cell as a yearly index of seasonal asynchrony between R_s and plant fixation of CO₂. GSNF is defined as the cumulative NEP over the period of months for which NEP is positive. It reflects the magnitude in net forcing of seasonal variations in atmospheric CO₂ from the terrestrial biosphere.

Among relatively undisturbed land cover types, the TMF class has a comparatively low average GSNF at 67 g C m⁻² growing season⁻¹, in contrast to average GSNF in savanna and seasonal woodland areas of around 100 g C m⁻² (Table 2a). The model prediction of GSNF is consistently highest (> 100 g C m⁻² growing season⁻¹) in areas of Brazil classified as converted or cultivated, suggesting a greater seasonal separation between NPP and R_s . This pattern leads to the hypothesis that land use change and human modification has a significant effect of seasonal timing of plant growth and associated carbon fixation.

Soil carbon storage

Based on the near steady-state NASA-CASA model predictions, we find that land cover classes defined by Stone *et al.* (1994) as converted or cultivated consistently show

soil C storage in surface layers 3% to 47% lower on average than their relatively undisturbed land cover equivalents (Table 2a). This range is similar to those reported in previous studies of the effects of land cover change on soil carbon pools in the tropics (Allen 1985; Cerri *et al.* 1985; Davidson & Ackerman 1993).

For comparison to NASA-CASA model estimates, the soil map in our Amazon GIS was adapted to show percentage carbon content to g C m⁻³ storage separately for the top soil layer (\approx 0–0.15 m depth) and subsoil layers (\approx 0.15–1-m depth) by adjustment using bulk density estimates for each soil group (Table 3). Our GIS-based total for Brazil in terms of carbon storage in surface soils layers is 106 Pg C to 1-m depth (Table 2a). More than 50% of this regional total is located in TMF ecosystems which, on average, is second only to the seasonally flooded Patanal wetland in terms of carbon storage per m² soil area. Our mean value of 15.5 kg C m⁻²–1-m depth estimated for TMF closely matches predicted values by McKane *et al.* (1995) using the MBL-General Ecosystem Model (GEM) across a transect of Amazon forest sites. Expressed in terms of soil groups (Table 3), podzols and hydromorphic oxisols show the highest pool sizes for mean carbon storage per m² soil area. Ultisols have slightly higher pool size on average than oxisols, which also reflects the predicted trend in annual NPP.

For the legal Amazon region alone, total carbon storage from our GIS-based analysis is almost 40% higher than reported in previous regional inventory studies (Moraes *et al.* 1995). Our regional estimate is 74 Pg C stored to 1-m depth, compared to the estimate by Moraes *et al.* (1995) of 47 Pg C. One explanation for the difference is that the approach of Moraes *et al.* (1995) apparently averages out the soil profile estimates for both percentage C and bulk density by soil type, which eliminates the extremes in the soil survey dataset. Our interpolation of pit profile attributes within mapped soil groups under the criteria of nearest-neighbour similarity of profile soil classification to the closest matching soil group should preserve the full range of measured percentage carbon values in the original RADAMBRASIL records (MME 1981). Consequently, the method we used in this study to calculate soil C storage in surface layers is designed to minimize averaging of C storage capacity across any given soil type. For example, our mapping method shows areas with storage to 1-m at greater than 30 kg C m⁻², whereas the highest comparable value in the Moraes *et al.* (1995) map version is reported to be 22 kg C m⁻². Neither map version can be verified at this time, so that the contrasting results merely represent a possible range of total carbon storage for the legal Amazon region. Furthermore, additional measurement and simulation work is required to address the impacts of land use

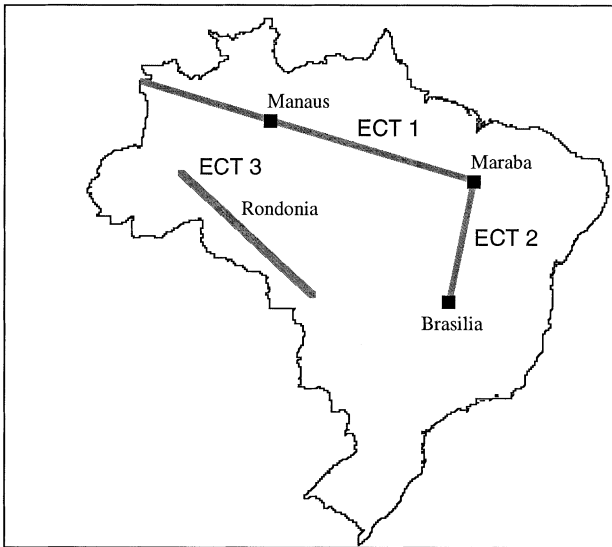


Fig. 8 Eco-climatic transects in Brazil (after LBA Science Planning Group 1996)

changes on soil carbon storage, which cannot be captured in static mapping analyses.

Our model results from NASA-CASA can be used in combination with the GIS soils data to estimate the portion of total soil C storage in surface layers to 1-m depth that has a residence time in the ecosystem on the order of several decades or less (Potter & Klooster 1997). This 'modern' soil C pool is represented principally by the predicted size of the model's SLOW pool (Table 2a), defined as the soil C reservoir in near-steady state exchange with plant production and decomposition on time scales of decades. We assume that the majority of the SLOW soil pool is stored at 0.2–0.3 m depth (Parton *et al.* 1992), although, in theory, the model estimate could extend to the full rooting depth of 1–2 m at each grid cell.

Within the TMF class, we find that more than 20% of the total C in surface layers (to 1-m depth) typically resides in modern form. These model estimates are in fairly good agreement with measurements of modern carbon content, and turnover time of the fastest (active) pools in soils profiles of eastern Amazon forests, determined using carbon isotope methods (Trumbore *et al.* 1995). Expressed in terms of soil groups (Table 3), ultisols typically have a lower proportion of soil C in modern form than do oxisols. The explanation for this pattern may be related to the mapping of ultisols to a more sandy surface horizon whereas the oxisols often have more clay in surface horizons, although there are many exceptions to the generalization.

Soil NO and N₂O emissions

Estimated annual emission rates of NO from soils largely fall in the range of 100–400 mg N-NO m⁻² y⁻¹ across the

Brazilian region. Highest rates (> 500 mg N-NO m⁻² y⁻¹) are located in agricultural, converted or secondary seasonal deciduous forest areas (Table 2b), mostly in the eastern and southern extremes of the country. These are generally areas that have coarse to medium-coarse texture soils, moderate to high annual NPP, and extended length of the dry season (i.e. longer than two months). Fertilizer sources of N are not included in these flux rates.

Intra-annual patterns in soil NO emission rates suggest that seasonal deciduous forest and savanna-woodland areas typically have highest emission rates in July–October. This seasonal pattern, and the typical range emissions of 100–400 mg N-NO m⁻² y⁻¹, are both in good agreement with short-term flux rates reported previously at field sites in the tropics (Hao *et al.* 1988; Kaplan *et al.* 1988; Bakwin *et al.* 1990; Davidson *et al.* 1991; Cardenas *et al.* 1993; Davidson & Kinglerlee 1997). In comparison, annual emission rates for soil N₂O average around 70 mg N-N₂O m⁻² y⁻¹ in seasonal deciduous forests and savanna, but can exceed 150 mg N-N₂O m⁻² y⁻¹ in moist forest areas.

The ratio of annual N₂O to NO flux is estimated at 0.5 over the entire country (Table 2b), which reflects the regional mapping results of sandy surface soils, periodic dry spells and coinciding litterfall (i.e. mineralization substrate availability) throughout the region. Within the TMF area, the N₂O:NO ratio is generally higher than the national average. Because of the influence of texture (Fig. 3), there may also be an effect of soil type on N₂O:NO, with average ratio for ultisols estimated at 0.4 and oxisols at 0.7, because the ultisols have higher sand content on average.

The model probably underestimates actual emission rates of N₂O from soils in Amazon forests. Among the most important reasons for this may be that our generalized model algorithms for soil moisture retention capacity and drainage rates are not yet well-adapted to tropical soil types. Another possibility is the problem of rooting depth settings. If Amazon vegetation can extract moisture from throughout a deep profile, the top soil layers would not dry out as rapidly, as predicted by the model, leading to higher residual moisture content that would promote N₂O over NO emission.

Eco-climatic transects

Transects are proposed for ecological field studies in the Amazon to represent gradients in precipitation, superimposed on varying soil types and land uses, including forest conversion, pasture management, or selective logging (LBA 1996). Selected eco-climatic transects (ECT) of interest are located along lines roughly connecting the following points: (1) Amazonia west of Manaus to Marabá, (2) Marabá to Brasília, (3) northern Rondônia to

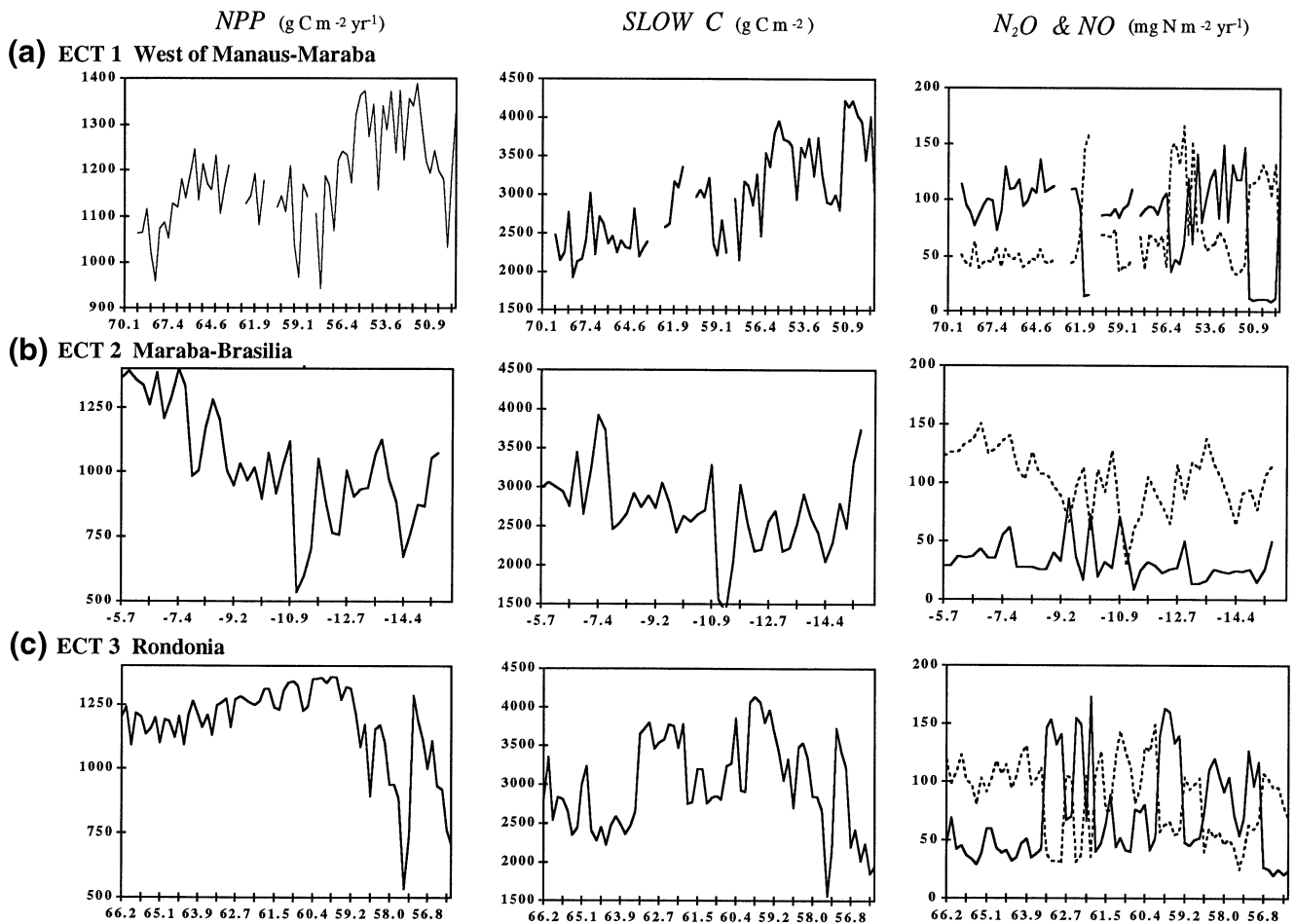


Fig. 9 Predicted patterns in net primary production, soil (SLOW) carbon storage, and nitrogen trace gas emissions (N_2O solid line, NO dashed line) along the selected eco-climatic transects.

central Mato Grosso (Fig. 8). Average rainfall at the western extreme of ECT 1 is about 1.8–2.0 m y^{-1} , whereas it averages around 1.5 m y^{-1} at the southern end of ECT 2. Rainfall at the north-western end of ECT 3 averages about 2.2 m y^{-1} , while it is about 1.2 m y^{-1} at the south-eastern extreme.

Our model estimates along these hypothetical transects suggest that NPP at relatively undisturbed sites increases markedly from west to east along the full extent of ECT 1, largely as a result of increasing average solar radiation (Fig. 9a). NPP decreases from north to south along ECT 2 as a consequence of decreasing rainfall (Fig. 9b); the length of the dry season increases steadily from two to five months along ECT 2. Carbon content in the modern (SLOW) pool tracks patterns in NPP to a degree, with differences resulting from variations in soil type and land use. As expected, the $N_2O:NO$ emission ratio decreases moving from wet to dry climate zones, although model results suggest that variations in soil texture (Fig. 4b.)

may also play a significant role in determining N trace gas emissions along these transects.

While we could detect no clear trends in model results along the entire length of ECT 3 (Fig. 9c), this area reveals important potential effects of land use on ecosystem production and biogeochemistry. Over most of the western portion of the transect, both annual NPP and the SLOW C pool increase modestly from north-west to south-east, until the point near 60° W where typical length of the dry season reaches three months duration (and mean rainfall is less than 1.6 m y^{-1}). At this point, TMF production is reduced sharply. Eastward of 60° W, notable reductions (10–15%) in FA-NDVI and NPP can be associated with adjacent grid cells classified as CMF (Stone *et al.* 1994). Although N trace gas fluxes appear highly variable, predominance of N_2O over NO flux is predictable – the estimated $N_2O:NO$ ratio can increase to greater than 4.5 at locations where fine texture soils are located.

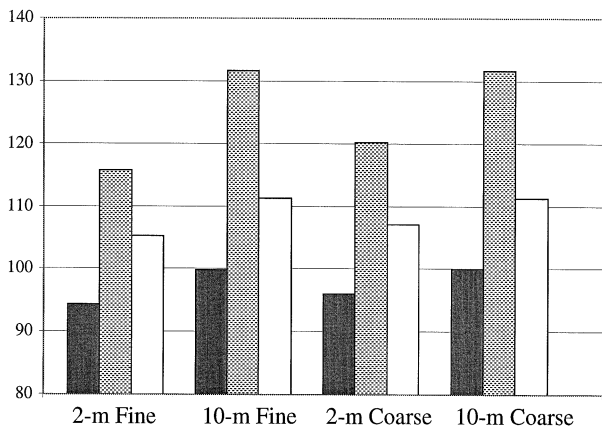


Fig. 10 Sensitivity in model estimates of the water stress scalar (W) for net primary production (NPP) (dark bars; percentage), estimated evapotranspiration (light bars, mm mo^{-1}), and NPP (white bars; $\text{g C m}^{-2} \text{y}^{-1}$). Groups are by potential rooting depth (2 m or 10 m) and soil texture (fine or coarse-medium).

Sensitivity tests

Simulation tests for a field site location in the eastern Amazon, near the city of Paragominas ($2^{\circ}59'S$, $47^{\circ}31'W$) in the state of Pará were conducted to address the potential importance of soil rooting depth and texture settings in the model. The deeply weathered clay soils at the site are common throughout the Amazon region (Nepstad *et al.* 1994). Tree roots have been found in soil shafts to greater than 10 m depths, and it is probable that evergreen forest canopies are maintained during the extended dry season by absorbing soil water stored to this depth and below. Our model driver for FA-NDVI at this forest grid cell location shows only a 12% decline during the driest months (July through November) from the peak FA-NDVI value in June, which is in close agreement with measured seasonal changes in leaf area at the Paragominas forest site (Nepstad *et al.* 1995). This is in contrast to savanna areas to the south that show more than a 30% decline in FA-NDVI from peak values to the driest months.

Comparison of model results from four simulations, with rooting depth settings at either 2 m or 10 m for either fine or coarse-medium texture soil conditions, shows that estimated monthly NPP of the primary forest increases by almost 6% on average when the deep rooting depth (10 m) is set (Fig. 10). Change in soil texture affects NPP to a lesser degree (< 2% increase with the coarse-medium setting) under either setting for rooting depth. These difference patterns in production estimates among the four simulation settings are also seen in estimated evapotranspiration (EET) and the model's water stress scalar (W) for plant production. To also test the model sensitivity to potential land cover change in the area, we repeated the NPP simulation with pasture settings that

include 1-m rooting depth and fine soil texture. These results show that pasture NPP decreases by 24% compared to the yearly primary forest NPP estimate (2-m rooting depth). Under hypothetical drought conditions of 50% lower annual rainfall, yearly NPP for a pasture would decrease 36% whereas NPP in the primary forest would decrease only 18%, relative to forest NPP under mean annual rainfall levels.

Soil texture has a much greater effect on estimates of soil moisture content (as WFPS) and nitrogen trace gas emission, compared to its relatively moderate influence on plant production. Regardless of rooting depth, the change from fine texture soil to coarse-medium texture reduces WFPS from values typically estimated at higher than 80% year-round to consistently lower than 50% WFPS. This results primarily from calibration of lower moisture retention capacity in sandy soils. Consequently, the predicted $\text{N}_2\text{O}:\text{NO}$ emission ratio changes from greater than 12 in fine texture soil to less than 0.4 in coarse-medium texture soil under either rooting depth. The deep rooting depth (10 m) setting increases the average WFPS by less than 20% in both soil texture cases, to a level that results in a zero estimated emission of NO in fine texture soil.

Summary

In any ecosystem modelling study, it is practically impossible to validate many predictions from local and regional scale simulations (Oreskes *et al.* 1994). Significant uncertainties remain in both the reliability of geographical datasets used to drive the model, and in the algorithms used to scale-up ecosystem processes and estimated carbon and nutrient fluxes. Nevertheless, our simulation model results suggest several key hypotheses that may be tested in subsequent experimental and remote sensing studies of Amazon ecosystems and biogeochemistry.

- 1 Solar radiation intercepted by persistent cloud cover over the Amazon basin is a primary limiting factor to evergreen forest NPP where the dry season typically does not last for more than one or two months.
- 2 Deep rooting and drought tolerance by trees in seasonally dry evergreen forests of the Amazon maintains primary production during dry seasons that typically last for more than two months.
- 3 Under conditions of similar seasonal rainfall and surface irradiance, the vegetation of converted forest lands is less productive on an annual basis than are relatively undisturbed forests in the Amazon region, mainly because of the lower tolerance to drought of pasture and crop plants relative to the forest trees they are replacing.
- 4 Total soil carbon storage covaries with annual NPP across the Amazon basin within broad texture classes,

and hence will change as land cover alters ecosystem production.

5 Soil texture is the dominant controller of N₂O:NO emission ratio over extensive areas of the Amazon basin.

Acknowledgements

This research was funded through grants from the National Science Foundation (TECO #9524050), and from NASA's program in Terrestrial Ecology and Modelling. The Foundation of California State University Monterey Bay provided additional support to the first author. We thank Sieste Los for assistance in the application of FAS algorithms. Tom Stone provided guidance on vegetation class definitions. Brad Lobitz assisted with spatial interpolation algorithms.

References

- Agbu PA, James ME (1994) NOAA/NASA Pathfinder AVHRR Land Data Set User's Manual. Goddard Distributed Active Archive Center, NASA Goddard Space Flight Center, Greenbelt.
- Allen JC (1985) Soil response to forest clearing in the United States and the tropics: geological and biological factors. *Biotropica*, **17**, 15–27.
- Bakwin PS, Wofsy SC, Fan S, Keller M, Trumbore SE, da Costa JM (1990) Emission of nitric oxide (NO) from tropical forest soils and exchange of NO between the forest canopy and atmospheric boundary layers. *Journal of Geophysical Research*, **95**, 16,755–15,764.
- Birkeland PW (1974) *Pedology, Weathering and Geomorphological Research*. Oxford University Press, New York, 285 pp.
- Bishop JKB, Rossow WB (1991) Spatial and temporal variability of global surface solar irradiance. *Journal of Geophysical Research*, **96**, 16,839–16,858.
- Cardenas L, Rondon A, Johansson C, Sanhueza E (1993) Effects of soil moisture, temperature, and inorganic nitrogen on nitric oxide emissions from acidic tropical savannah soils. *Journal of Geophysical Research*, **98** (D8), 14,783–14,790.
- Cerri CC, Feller C, Balesdent J, Victoria R, Plenecassagne A (1985) Application du traçage isotopique naturel en ¹³C, a l'étude de la dynamique de la matière organique dan les sols. *Compte Rendus de l'Académie des Sciences, Paris, Série II*, **300**, 423–428.
- Davidson EA (1991) Fluxes of nitrous and nitric oxide from terrestrial ecosystems. In: *Microbial Production and Consumption of Greenhouse Gases: Methane, Nitrogen Oxides and Halomethanes* (eds Rogers JE, Whitman WB), pp. 219–235. American Society for Microbiology, Washington, DC.
- Davidson EA (1993) Soil water content and the ratio of nitrous oxide to nitric oxide emitted from soil. In: *Biogeochemistry and Global Change: Radiatively Active Trace Gases* (ed. Oremland RS), pp. 369–386. Chapman and Hall, New York.
- Davidson EA, Ackerman IL (1993) Changes in soil carbon inventories following cultivation of previously untilled soils. *Biogeochemistry*, **20**, 161–193.
- Davidson EA, Kinglerlee W (1997) A global inventory of nitric oxide emissions from soils. *Nutrient Cycling in Agroecosystems*, **48**, 91–104.
- Davidson EA, Vitousek PM, Matson PA, Riley R, Garcia-Mendez G, Maass JM (1991) Soil emissions of nitric oxide in a seasonally dry tropical forest of Mexico. *Journal of Geophysical Research*, **96** (D8), 15,439–15,445.
- DCW (1993) *Digital Chart of the World: for Use with ARC/INFO Software*. Environmental Systems Research Institute, Inc., Redlands, CA.
- DeFries R, Townshend J (1994) NDVI-derived land cover classification at global scales. *International Journal of Remote Sensing*, **15**, 3567–3586.
- Firestone M, Davidson E (1989) Microbial basis of NO and N₂O production and consumption. In: *Exchange of Trace Gases Between Ecosystems and the Atmosphere* (eds Andreae MO, Schimel DS). Wiley/ Dahlem Konferenzen.
- Food and Agricultural Organization (FAO) /UNESCO (1971) Soil Map of the World. 1:5 000 000. United Nations Educational, Scientific, and Cultural Organization, Paris.
- Gordon HR, Brown JW, Evans RH (1988) Exact Rayleigh scattering calculations for use with the Nimbus-7 coastal zone color scanner. *Applied Optics*, **27**, 2111–2122.
- Grace J, Lloyd J, McIntyre J, Miranda AC, Meir P, Miranda HS, Nobre C, Moncrieff J, Massheder J, Malhi Y, Wright I, Gash J (1995) Carbon dioxide uptake by an undisturbed rain forest in southwest Amazonia. *Science*, **270**, 778–780.
- Hao WM, Scharffe D, Crutzen PJ (1988) Production of N₂O, CH₄ and CO₂ from soils in the tropical savanna during the dry season. *Journal of Atmospheric Chemistry*, **7**, 93–105.
- Holben BN (1986) Characteristics of maximum-value composite images from temporal AVHRR data. *International Journal of Remote Sensing*, **7**, 1417–1434.
- Hutchinson GL, Davidson EA (1993) Processes for production and consumption of gaseous nitrogen oxides in soil. In: *Agricultural Ecosystem Effects on Trace Gases and Global Climate Change*. American Society of Agronomy, Special Publication no. 55, Madison, WI, pp. 79–93.
- IBGE/IBDF. (1988) *Mapa de Vegetação do Brasil*. Ministerio da Agricultura, Brasilia.
- Jipp PH, Nepstad DC, Cassel DK, Reis de Cavalho C (1997) Deep soil moisture storage and transpiration in forests and pastures of seasonally dry Amazonia. *Climatic Change*.
- Kaplan WA, Wofsy SC, Keller M, da Costa JM (1988) Emission of NO and deposition on O₃ in a tropical forest system. *Journal of Geophysical Research*, **93**, 1389–1395.
- Keller ME, Reiners WA (1994) Soil-atmosphere exchange of nitrous oxide, nitric oxide and methane under secondary forest succession of pastures to forest in the Atlantic lowlands of Costa Rica. *Global Biogeochemical Cycles*, **8**, 399–409.
- Kidwell K (1991) *NOAA Polar Orbiter Data User's Guide*. NCDC/SDSD. National Climatic Data Center, Washington, DC.
- LBA Science Planning Group. (1996) *The Large Scale Biosphere-Atmosphere Experiment in Amazonia (LBA): Concise Experimental Plan*. Cachoeira Paulista, SP, Brazil, 44pp.
- Linn DM, Doran JW (1984) Effect of water-filled pore space on carbon dioxide and nitrous oxide production in tilled and nontilled soils. *Soil Society of America Journal*, **48**, 1267–1272.

- Los SO, Justice CO, Tucker CJ (1994) A global 1x1 NDVI data set for climate studies derived from the GIMMS continental NDVI data. *International Journal of Remote Sensing*, **15**, 3493–3518.
- Lucas RM, Curran PJ, Honzak M, Foody GM, do Amaral I, Amaral S (1996) Disturbance and recovery of tropical forests: balancing the carbon account. In: *Amazonian Deforestation and Climate* (eds Gash JHC, Nobre CA, Roberts JM, Victoria RL), pp. 384–398. Wiley, Chichester, UK.
- Manrique LA, Jones CA (1991) Bulk density of soils in relation to soil physical and chemical properties. *Soil Science Society of America Journal*, **55**, 476–481.
- Matson PA, Vitousek PM (1990) An ecosystem approach to the development of a global nitrous oxide budget. *Bioscience*, **40**, 677–672.
- McKane RB, Rastetter EB, Melillo JM, Shaver GR, Hopkinson CS, Fernandes DN, Skole DL, Chomentowski WH (1995) Effects of global change on carbon storage in tropical forests of South America. *Global Biogeochemical Cycles*, **9**, 329–350.
- Ministério das Minas e Energia (MME). (1981) *Projeto Radambrasil*. Rio De Janeiro, Brazil.
- Monteith JL (1972) Solar radiation and productivity in tropical ecosystems. *Journal of Applied Ecology*, **9**, 747–766.
- Moraes JL, Cerri CC, Melillo JM, Kicklighter D, Neill C, Skole DL, Steudler PL (1995) Soil carbon stocks of the Brazilian Amazon basin. *Soil Science Society of America Journal*, **59**, 224–247.
- Negreiros GH, Nepstad DC (1994) Mapping deeply-rooting forests of Brazilian Amazonia with GIS. Proceedings of ISPRS Commission VII Symposium, Rio de Janeiro. *Resource and Environmental Monitoring*, **7(a)**, 334–338.
- Nepstad D, de Carvalho CR, Davidson E, Jipp P, Lefebvre P, Negreiros GH, da Silva ED, Stone T, Trumbore S, Vieira S (1994) The role of deep roots in the hydrologic and carbon cycles of Amazonia forests and pastures. *Nature*, **372**, 666–669.
- Nepstad D, Jipp P, Moutinho P, Negreiros GH, Vieira S (1995) Forest recovery following pasture abandonment in Amazonia: Canopy seasonality, fire resistance, and ants. In: *Evaluating and Monitoring the Health of Large-Scale Ecosystems* (eds Rappaport DJ, Gaudet CL, Calow P). NATO ASI Series, Vol. 128, pp. 333–349. Springer-Verlag, Berlin.
- Nobre CA, Gash JHC, Roberts JM, Victoria RL (1996) Conclusions from ABRACOS. In: *Amazonian Deforestation and Climate* (eds Gash JHC, Nobre CA, Roberts JM, Victoria RL), pp. 577–595. Wiley, Chichester, UK.
- Oreskes N, Shrader-Frechette K, Belitz K (1994) Verification, validation, and confirmation of numerical models in the earth sciences. *Science*, **263**, 641–646.
- Papendick RI, Campbell GS (1980) Theory and measurement of water potential. In: *Water Potential Relations in Soil Microbiology*, pp. 1–22. Soil Science Society of America, Madison, WI.
- Parton WJ, McKeown B, Kirchner V, Ojima D (1992) *Century Users Manual*. Natural Resource Ecology Laboratory, Colorado State University, Fort Collins, CO.
- Parton WJ, Schimel DS, Cole CV, Ojima DS (1987) Analysis of factors controlling soil organic matter levels in Great Plains grasslands. *Soil Science Society of America Journal*. **51(5)**, 1173–1179.
- Potter CS, Klooster SA, Brooks V (1997) Interannual variability in terrestrial net primary production: Exploration of trends and controls on regional to global scales. *NASA Workshop on Interannual Biosphere-Atmosphere Variability*, March 24–26, 1997, Tucson, AZ.
- Potter CS, Klooster SA, Chatfield RB (1996) Consumption and production of carbon monoxide in soils: A global model analysis of spatial and seasonal variation. *Chemosphere*, **33** (6), 1175–1193.
- Potter CS, Klooster SA (1997) Global model estimates of carbon and nitrogen storage in litter and soil pools: response to changes in vegetation quality and biomass allocation. *Tellus*, **49B**, 1–17.
- Potter CS, Matson PA, Vitousek PM, Davidson EA (1996) Process modeling of controls on nitrogen trace gas emissions from soils world-wide. *Journal of Geophysical Research*, **101**, 1361–1377.
- Potter CS, Randerson JT, Field CB, Matson PA, Vitousek PM, Mooney HA, Klooster SA (1993) Terrestrial ecosystem production: A process model based on global satellite and surface data. *Global Biogeochemical Cycles*, **7** (4), 811–841.
- Riley RH, Vitousek PM (1995) Nutrient dynamics and nitrogen trace gas flux during ecosystem development in montane rain forest. *Ecology*, **76**, 292–304.
- Roberts J, Cabral OMR (1993) ABRACOS: a comparison of climate, soil moisture, and physiological properties of forests and pastures in the Amazon Basin. *Commonwealth Forestry Review*, **72**, 310–315.
- Root TL, Schneider SH (1995) Ecology and climate: Research strategies and implications. *Science*, **269**, 334–341.
- Schuster M, Conrad R (1993) Metabolism of nitric oxide and nitrous oxide during nitrification and denitrification in soil at different incubation conditions. *Microbiology Ecology*, **101**, 133–143.
- Sellers PJ, Tucker CJ, Collatz GJ, Los SO, Justice CO, Dazlich DA, Randall DA (1994) A global 1x1 NDVI data set for climate studies. Part 2: the generation of global fields of terrestrial biophysical parameters from the NDVI. *International Journal of Remote Sensing*, **15**, 3519–3545.
- Shuttleworth WJ (1988) Evaporation from Amazonian forest. *Proceedings of the Royal Society of London, Series B*, **233**, 321–346.
- Skole D, Tucker C (1993) Tropical deforestation and habitat fragmentation in the Amazon: Satellite data from 1978 to 1988. *Science*, **260**, 1905–1910.
- Stone TA, Schlesinger P, Houghton RA, Woodwell GM (1994) A map of vegetation of South America based on satellite imagery. *Photogrammetric Engineering and Remote Sensing*, **60**, 541–551.
- Thorntwaite CW (1948) An approach toward rational classification of climate. *Geographical Reviews*, **38**, 55–94.
- Trumbore SE, Davidson EA, de Camargo PB, Nepstad DC, Martinelli LA (1995) Belowground cycling of carbon in forests and pastures of eastern Amazonia. *Global Biogeochemical Cycles*, **9**, 515–528.